Nonisothermal Healing and Interlaminar Bond Strength Evolution During Thermoplastic Matrix Composites Processing

F. YANG *and* R. PITCHUMANI*

Composites Processing Laboratory
Department of Mechanical Engineering
University of Connecticut
Storrs, CT 06269-3139

Thermoplastic-matrix composite products are fabricated by applying heat and pressure to contacting thermoplastic surfaces, and consolidating the interface. The combined processes of interfacial contact area increase, referred to as intimate contact, and polymer interdiffusion (healing) across the interfacial areas in contact are responsible for the development of interlaminar bond strength in the composite products. In this paper, a model for the healing process under nonisothermal conditions is presented starting from a fundamental formulation of the reptation of polymer chains. The healing model is coupled with an intimate contact model based on a fractal representation of the asperity structures on thermoplastic tow surfaces, to provide a comprehensive description of the interfacial bond strength evolution during nonisothermal processing. Nondimensional analysis is used to identify the ranges of a parameter, introduced as the *fusion bonding number*, which correspond to the interfacial bonding process being healing-limited, intimate-contact-limited, or equally dominated by both mechanisms.

1. INTRODUCTION

Processing of thermoplastics and thermoplastic-based composites using techniques such as tow placement, tape laying, resistance welding, and autoclave forming is governed by the principle of fusion bonding, which involves applying heat and pressure to the interface between two contacting material layers. The softened materials at the elevated temperatures are spread by the applied pressure, forming close contact between the adjacent layers—a process referred to as intimate contact—followed by the interdiffusion of polymer chains across the area in contact—a process referred to as healing. The processes of intimate contact and healing are coupled in that healing can occur only across areas of the interface that are in intimate contact. While intimate contact development is a function of the applied pressure, temperature, and time, healing is governed by the temperature history and time alone. As a result of the coupling, however, the interlaminar bond strength, σ, is a function of the processing temperature, T, the consolidation pressure, p, and the processing time, t (1–9).

$$\sigma = f(T, p, t) \tag{1}$$

Isothermal healing of a polymer interface via molecular interdiffusion is often described using the reptation theory, which models the motion of individual linear polymer chains in amorphous bulk (10, 11). In the model, a polymer chain of length L is considered to be confined to a tube, which represents the steric effects of neighborhood chains (*Fig. 1*). The tube forms a geometric constraint such that the chain can only move along its curvilinear length. At the beginning of the process, $t = 0$, the chain, represented by the thin solid line in *Fig. 1*, is totally encompassed by the original tube. The chain moves within the tube in a Brownian motion manner, and after a period of time, the chain ends escape from the original tube, forming the "minor chains." The length, ℓ, of the minor chains increases with time and reaches L at the reptation time t_R (when the entire polymer chain escapes from the tube). Considering an interface between two thermoplastic layers in perfect contact, as time proceeds and as the lengths of the minor chains grow, some of the chains from each layer move across the interface, and

*To whom correspondence should be addressed.
(Email: r.pitchumani@uconn.edu)

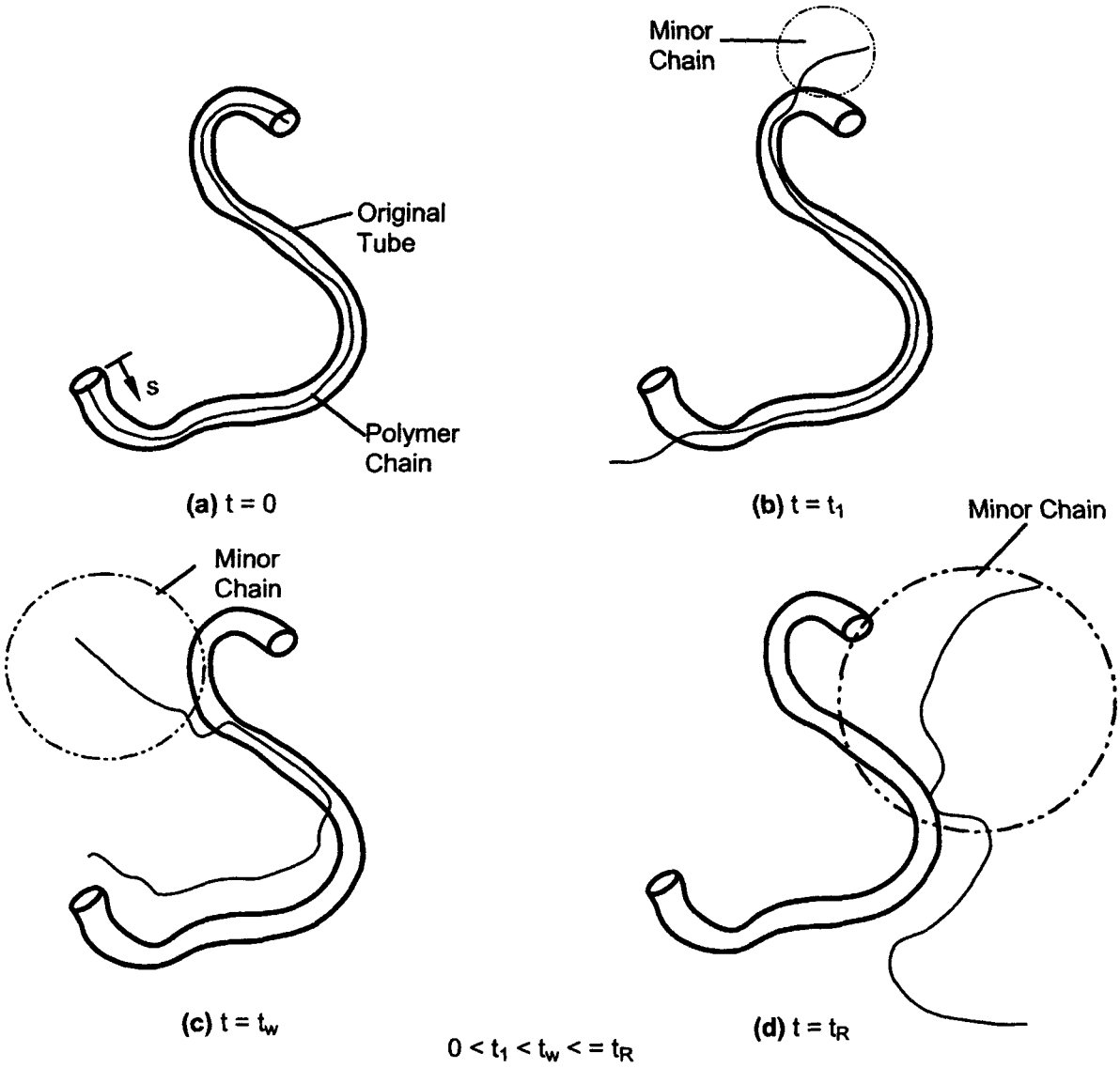

Fig. 1. The reptation movement of a linear polymer chain in an entangled melt. The chain escapes from its original tube at the reptation time, t_R [redrawn from ref. (1)].

the net interpenetration depth, χ, contributes to the bond strength buildup. After the reptation time, the interpenetration and entanglement of all the polymer chains are fully developed and the molecular configuration at the interface is identical to that of the virginal bulk material.

The interlaminar bond strength, σ, is proportional to the interpenetration distance χ, which is related to the minor chain length as $\chi \sim \sqrt{\ell}$, by considering the minor chains to amble across the interface via a random walk motion (2). The ultimate bond strength, σ_∞, is achieved as the interpenetration depth and the minor chain length reach their maximum values, χ_∞ and L, respectively. A degree of healing may be defined as the ratio of the instantaneous interfacial bond strength to the ultimate bond strength as (10, 11):

$$D_h(t) = \frac{\sigma}{\sigma_\infty} = \frac{\chi}{\chi_\infty} = \left(\frac{\ell}{L}\right)^{\frac{1}{2}} \tag{2}$$

Note that *Eq 2* applies to isothermal and nonisothermal conditions alike; however, the growth of the minor chain length with time, which is governed by a diffusion process of polymer chains, depends on the temperature history. Under isothermal conditions, in which the diffusion coefficient for a given polymer chain is likely to be a constant, the evolution of the minor chain length, ℓ, with time $t < t_R$ is expressed as (1, 10)

$$\frac{\ell}{L} = \left(\frac{t}{t_R}\right)^{1/2} \tag{3}$$

From *Eqs 2* and *3* it follows that, under isothermal conditions, the degree of healing is given by

$$D_h(t) = \frac{\sigma}{\sigma_\infty} = \left(\frac{t}{t_R}\right)^{\frac{1}{4}} \quad (4)$$

in which the reptation time, t_R, a function of temperature, may be described by an Arrhenius type equation (5) or other empirical means (4).

Bastien and Gillespie (12) extended the isothermal healing model (*Eq 4*) to nonisothermal fusion bonding of amorphous thermoplastic laminates. In their model development, the temporal domain of a non-isothermal healing process was divided into q time intervals ($t_{i+1} - t_i = \Delta t = t/q$), and the process in each ith interval was considered to be isothermal at the average of the temperatures between t_i and t_{i+1}. The incremental bond strengths accrued within each Δt were derived from the isothermal reptation theory and the intent of the model was to determine the bond strength at any instant t as the summation of the incremental values.

$$D_h(t) = \frac{\sigma}{\sigma_\infty} = \sum_{i=0}^{t/\Delta t}\left[\frac{t_{i+1}^{1/4} - t_i^{1/4}}{t_R^{*1/4}}\right] \quad (5)$$

The foregoing nonisothermal extension of the healing model seemingly appears plausible, and in fact has been widely accepted and used in modeling fabrication processes (5, 6, 13). However, a closer examination of the model reveals that the expression reported for the incremental bond strengths during each ith time interval, i.e., the term within square brackets in *Eq 5*, is truly valid only if the process were isothermal at the average temperature T_i^* from $t = 0$ to $t = t_{i+1}$, for each i. Since this does not represent the thermal history during actual processing conditions, the model is strictly inappropriate for a nonisothermal process.

Sonmez and Hahn (14) modified the isothermal reptation model using an approach similar to that of Bastien and Gillespie in order to simulate nonisothermal healing during thermoplastic composite tape placement. The incremental growth in the dimensionless minor chain length $\left(\frac{d\ell}{L}\right)$ during a time interval dt, was obtained by differentiating *Eq 3* with respect to time, and the total minor chain length at any time t was obtained by integrating the differential over the period from 0 to t to get a degree of healing under nonisothermal condition as

$$D_h(t) = \frac{\sigma}{\sigma_\infty} = \sqrt{\frac{\ell}{L}} = \left[\int_0^t \frac{d\tau}{2\sqrt{\tau \cdot t_R(\tau)}}\right]^{1/2} \quad (6)$$

The above integral has a similar drawback as that in the case of the Bastien and Gillespie model. When applying to a nonisothermal process at the time interval $[\tau, \tau + d\tau]$, the integrand in *Eq 6* is appropriate only if the process were isothermal with the reptation time $t_R(\tau)$ from $t = 0$ to $t = \tau$. Again, this does not represent the real temperature history.

The development of the above nonisothermal healing models also ignored an important limitation when using the reptation theory, *Eqs 2–4*. As pointed out by Wool and coauthors (1, 2, 15), these equations are valid only for low molecular weights, M, in the range of $M_c < M < 8M_c$, where M_c is the critical entanglement molecular weight. However, for typical engineering thermoplastics, the molecular weight range is $M > 8M_c$, and *Eqs 2–4* are not applicable.

It is evident from the foregoing discussion that at the present time, there is no reliable means of describing polymer healing under nonisothermal conditions usually encountered in processing. The primary objective of the present study is to fill this critical void by developing a fundamental description of nonisothermal healing, founded on a first-principles formulation of the polymer reptation process and which is applicable over a wide range of molecular weights of practical relevance. Starting from a description of the Brownian motion of a single polymer chain, an analytical relationship is derived to relate the bond strength evolution to the nonisothermal temperature history. The healing model is validated using experimental data on fusion bonding of PEEK specimen, and parametric studies are presented to illustrate the effects of temperature history on the healing development. Comparisons with the expressions of Bastien and Gillespie (12) and of Sonmez and Hahn (14), are provided to examine the accuracy of the healing models in the literature relative to the exact solution.

A second objective of the paper is to couple the processes of intimate contact and healing to provide a comprehensive description of the fusion bonding process and interfacial bond strength evolution under nonisothermal conditions. To this end, the healing model is combined with an intimate contact model developed previously in the literature. Nondimensional analysis of the coupled bonding model is presented to identify a critical dimensionless parameter, termed the fusion bonding number, that determines the primary mechanism governing the bond strength development. Healing-limited and intimate-contact-limited processing regimes, as well as conditions for which both processes are equally dominant are developed in terms of the fusion bonding number.

2. FUSION BONDING MODELS

2.1 Nonisothermal Healing Model

Before presenting the development of the nonisothermal healing model, a more general form of the isothermal healing model is introduced to address the molecular weight limitation mentioned in the previous section. At high molecular weights, the interpenetration depth and the minor chain length do not have to reach χ_∞ and L to obtain the maximum bond strength, σ_∞, which is achieved instead at the welding time, t_w ($< t_R$, as shown in *Fig. 1c*), at which χ and ℓ have the values of χ_w ($< \chi_\infty$) and L_w ($< L$), respectively. Based on the above consideration, an expression of the degree of healing is obtained using the parameters at the welding time as follows:

$$D_h(t) = \frac{\sigma}{\sigma_\infty} = \frac{\chi}{\chi_w} = \left(\frac{\ell}{L_w}\right)^{\frac{1}{2}} = \left(\frac{t}{t_w}\right)^{\frac{1}{4}} \quad (7)$$

Note that the above equation is valid for the full range of molecular weight because of the fact that in the low molecular weight range, $t_w = t_R$, $\chi_w = \chi_\infty$, $L_w = L$, and *Eq 7* reduces to the expression given by *Eq 4*. *Equation 7* is used as the basis to develop the nonisothermal healing model as follows.

Considering the description of the reptation motion of a polymer chain encased in a surrounding tube, a probability density function, $P(s, t)$, is defined as the probability of finding a particular chain segment at some position s at time t, where s is the curvilinear coordinate along the encompassing tube (*Fig. 1a*). The density function $P(s, t)$ was determined through a random walk analysis of the chain segments in the tube, and was shown to be mathematically governed by a diffusion equation (10, 11, 16)

$$\frac{\partial P}{\partial t} = D\frac{\partial^2 P}{\partial s^2} \quad (8)$$

where D is the reptation diffusion coefficient. Generally, the diffusivity D depends on the molecular weight, M, temperature, T, and hydrostatic pressure, p. For a typical polymer and its processing, M and p are constants, and the present focus is on the influence of the temperature, which is a function of time. Thus, for isothermal healing, the diffusion coefficient is a constant, whereas in the more general nonisothermal case, the diffusion coefficient is time-variant through its dependence on the temperature.

At time $t = 0$, the chain segment considered is at the origin, $s = 0$, and the initial condition associated with *Eq 8* may be written as:

$$P(s, 0) = \delta(0) \quad (9)$$

where δ is the Dirac delta function. The diffusion domain is considered to be infinitely large ($|s| \to \infty$), and since the chain segment will never be able to move across an infinite distance, the following natural boundary conditions must be automatically satisfied

$$P(s, t) = 0; \frac{\partial P(s, t)}{\partial s} = 0 \text{ as } |s| \to \infty \quad (10)$$

Under isothermal conditions ($T = T_0$), the reptation diffusivity $D_0 = D(T_0)$ is a constant, and the solution of *Eqs 8* and *9* is given as (11, 16)

$$P(s, t) = \frac{1}{[4\pi D_0 t]^{1/2}} \exp\left[-s^2/4D_0 t\right] \quad (11)$$

The mean-square displacement of the polymer chain at time t corresponds to the square of the minor chain length $\ell^2(t)$ and may be evaluated as follows using the isothermal probability density function (*Eq 11*).

$$\langle s^2 \rangle = \ell^2 = \int_{-\infty}^{+\infty} s^2 P(s, t) ds = 2D_0 t \quad (12)$$

Recall that the welding time for a given temperature is defined as the time required for the minor chain length to reach L_w, at which point, the maximum bond strength is obtained. From *Eq 12*, we may write

$$t_w(T_0) = \frac{L_w^2}{2D_0} \quad (13)$$

For an arbitrary temperature history, $T(t)$, the reptation diffusivity is a function of time, $D(t)$, and the nonisothermal bond strength evolution with time is obtained as solution of the governing equation, *Eq 8*, with a variable coefficient, and the associated conditions (*Eqs 9, 10*). The system of equations may be solved using the Fourier transformation or using the separation of variables technique (17). Omitting the details of the solution steps, which may be found elsewhere (18, 19), the probability density function can be obtained as

$$P(s, t) = \frac{1}{2\pi}\int_{-\infty}^{+\infty} \exp\left[\omega^2 \int_0^t -D(t)\, dt\right] \cos(\omega s)\, d\omega \quad (14)$$

Equation 14 forms the basis for nonisothermal healing analysis. It may be verified that for isothermal healing, *Eq 11* is recovered by setting $D(t) = D_0 = constant$ in *Eq 14*, and evaluating the resulting integrals.

Equation 13, which relates the welding time to the reptation diffusivity at any temperature, T, is used to replace the diffusion coefficient, $D(t)$, in terms of the welding time in *Eq 14*, as $D(t) = L_w^2/2t_w[T(t)]$. Furthermore, defining $f(t)$ for brevity as

$$f(t) = \int_0^t \frac{1}{2t_w} dt \quad (15)$$

the probability distribution function $P(s, t)$ (*Eq 14*) is evaluated as follows.

$$P(s, t) = \frac{1}{2\pi}\int_{-\infty}^{+\infty} \exp[-f(t)L_w^2\omega^2]\cos(\omega s)d\omega$$

$$= \frac{1}{\sqrt{4\pi f(t)L_w^2}} \exp[-s^2/4f(t)\, L_w^2]$$

Following *Eq 12*, the square of the minor chain length at time t for a nonisothermal temperature history is determined using the probability density function as

$$\begin{aligned} \ell^2(t) &= \int_{-\infty}^{+\infty} s^2 P(s, t)\, ds \\ &= \int_{-\infty}^{+\infty} s^2 \frac{1}{\sqrt{4\pi f(t) L_w^2}} \exp[-s^2/4f(t)L_w^2] ds \\ &= 2f(t)L_w^2 \end{aligned} \quad (16)$$

From *Eqs 7, 15*, and *16*, the nonisothermal degree of healing evolution with time is given by the following expression

$$D_h(t) = \left(\frac{\ell}{L_w}\right)^{1/2} = [2f(t)]^{1/4} = \left[\int_0^t \frac{1}{t_w(T)}dt\right]^{1/4} \quad (17)$$

The foregoing result is based on the solution of the fundamental equations governing reptation dynamics, and therefore constitutes a rigorous model for nonisothermal healing. For a given temperature history, and the temperature dependence of the welding time, the degree of healing can be evaluated using *Eq 17*. Note that for a constant temperature healing process, $t_w(T)$ is a constant, and the degree of healing reduces to the expression for isothermal healing given by *Eq 7*.

2.2 Intimate Contact Process Model

This section provides a brief review of the intimate contact process model reported in the literature, to set up the background information needed in the coupled bonding model described in the next two sections. A more comprehensive presentation of the process model is given in earlier references (8, 9). Recall that intimate contact refers to the development of interfacial contact area between thermoplastic plies, caused by the spreading of the surface asperities. The development of intimate contact is strongly influenced by the processing parameters—pressure, temperature, and time—and the surface geometric parameters. Modeling of the intimate contact process requires a quantitative description that captures the intrinsic features of the asperity structures on thermoplastic ply surfaces.

A model for intimate contact was presented by Dara and Loos (7), in which the thermoplastic surface asperity profiles were treated as a distribution of rectangular elements of different sizes. Lee and Springer (4) followed this model with a simplification of the geometry, taking the idealized rectangular elements to be of the same size. Although these models have been used to describe the processing of specific material systems, a principal limitation lies in the fact that the geometric parameters of the rectangular elements can not be determined directly from the surface profilometric measurements; the parameters are used as tuning factors to fit the model to experimental data.

A fundamental view of thermoplastic surfaces reveals that the geometric structure is random, and that the roughness features are found at a large number of length scales as shown in (8, 9). This suggests the existence of a fractal structure formed by the asperity elements, implying that when a portion of the asperity surface is magnified appropriately, the magnified structure will be statistically similar to the original (8, 9). A fractal geometry based description, which accounts for the roughness features at multiple length scales, may therefore be more appropriate for describing the surface asperities and their spreading process. Following this approach, Yang and Pitchumani (8) developed a fractal Cantor set construction to represent the multiscale asperity structures on thermoplastic ply surfaces. A squeeze flow model based on the fractal description was then developed to simulate the intimate contact evolution as a function of the process and surface geometric parameters.

The construction of a Cantor set surface, shown in *Fig. 2a*, is as follows: Starting from a rectangle of length L_0 and an arbitrary height, a small rectangle of height h_0 is removed from the middle, so that the remaining length of the rectangle is $L_1 = L_0/f$, where the scaling factor $f > 1$. This results in two identical rectangles of height h_0 and width $L_1/2$, which are called the first generation asperities. Next, from each of the first generation asperities, a rectangle of height $h_1 = h_0/f$ is removed, which yields four second-generation rectangular asperity elements of height h_1 and width $L_2/4$, where $L_2 = L_1/f$. Continuing the procedure results in the self-affine Cantor set in *Fig. 2a*.

The intimate contact process is modeled as the flattening of the Cantor set surface by a rigid half plane, as shown in *Fig. 2b*. The contact process starts with the squeeze flow of the highest generation asperities (theoretically, asperities at generation ∞), and progressively goes to the first generation asperities. When the asperities from the $(n + 1)$th generation are deformed, the (n)th and lower generations are supposed to retain their shape and all the deformed material is considered to flow into the troughs between the $(n + 1)$th generation asperities. When the troughs are completely filled, the rigid half plane has a cumulative displacement u_{n+1}, which is measured from the initial location of the Cantor surface as shown in *Fig. 2b*. The $(n + 1)$th generation asperities are then combined into the (n)th generation, and the process proceeds with the deformation of the (n)th generation asperities.

Based on the description of the Cantor set surface deformation process, the degree of intimate contact, $D_{ic}^{(n)}$ (defined as the fraction of the total surface area in contact at any time) for the (n)th generation asperities, was given by Yang and Pitchumani (8) as

$$D_{ic}^{(n)}(t) = \frac{1}{f^n}\left[\frac{5}{4}\left(\frac{h_0}{L_0}\right)^2 \frac{f^{\frac{2nD}{2-D}+n+4}}{(f+1)^2}\int_{t_{n+1}}^{t}\frac{p_{app}}{\mu}\,dt + 1\right]^{\frac{1}{5}},$$

$$t_{n+1} \le t \le t_n \quad (18)$$

where D is the fractal dimension of the thermoplastic surface, p_{app} is the applied gage pressure, μ is the viscosity of the material, and t_{n+1} and t_n are the start and end times for the consolidation process of the (n)th generation asperities, respectively. Note that the foregoing equation pertains to the (n)th generation asperities being in contact with the rigid flat plane. The degree of intimate contact evolution with time is obtained by recording the process from the highest generation (for which $t_{n+1} = 0$) down to the first. It must be pointed out that the geometric parameters in *Eq 18* can be completely determined from surface profile measurements (8), which eliminates the need for tuning the model to experimental data, as required in the other models in the literature (4, 7).

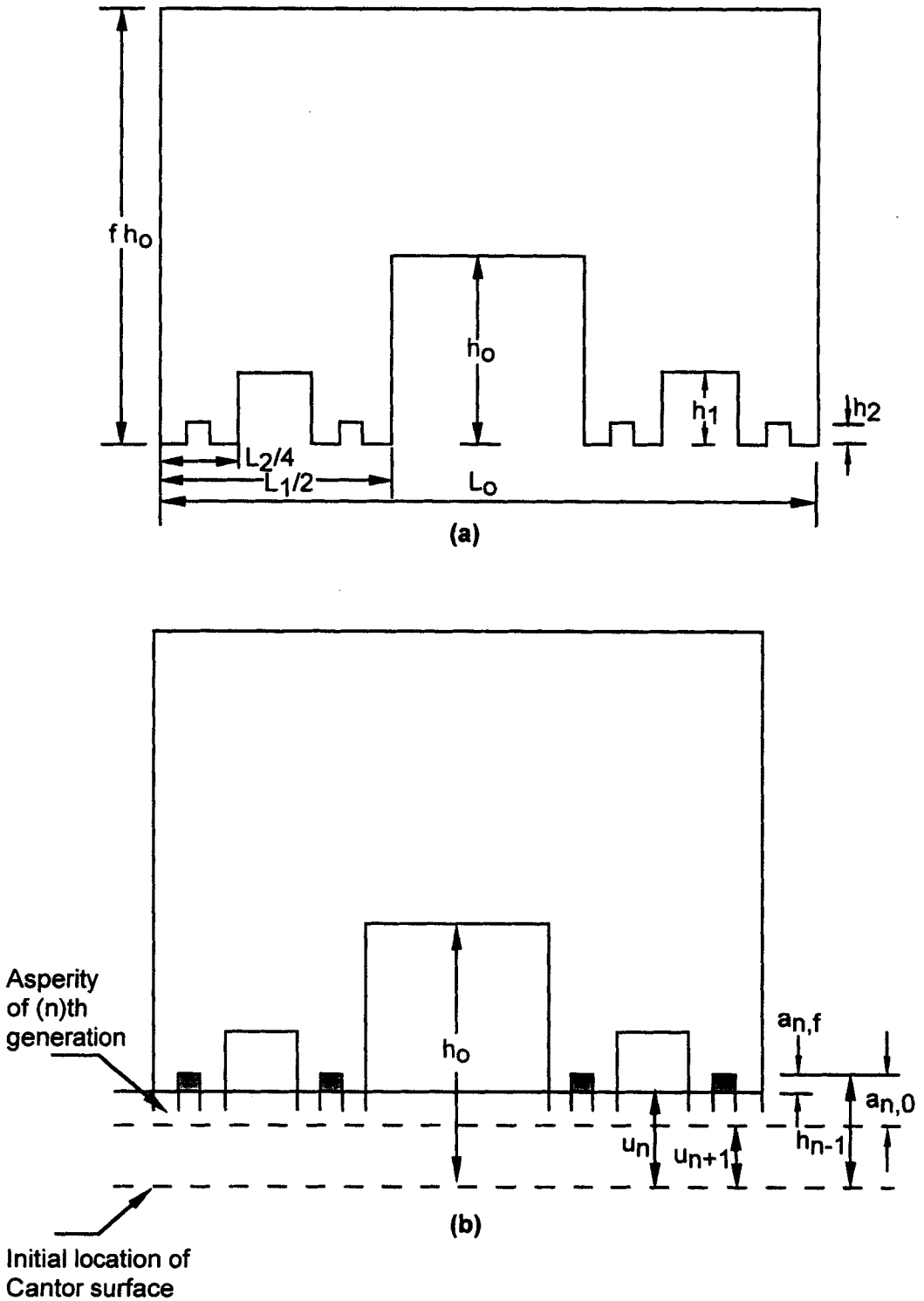

Fig. 2. (a) A Cantor set fractal representation of a thermoplastic surface and (b) deformation of a Cantor set surface by a contact plane.

2.3 The Coupled Bonding Model

Since polymer healing can take place only across interfacial areas in intimate contact, the interfacial bond strength is determined by the coupled effects of the two processes. At any time, t, during the fusion bonding process, an incremental intimate contact area, $(dD_{ic}/dt)dt$, develops at the interface. The degree of healing for this incremental area at the final bonding time, t_f, is denoted as $D_h(t_f - t)$, where $t_f - t$ represents the time available for the area to heal. The effective bond strength can therefore be expressed as an area average of the healing of all the incremental areas, and may be given in a non-dimensional form as the degree of bonding, D_b:

$$D_b(t_f) = D_{ic}(0) \cdot D_h(t_f) + \int_0^{t_f} D_h(t_f - t) \cdot \frac{dD_{ic}(t)}{dt} \cdot dt \tag{19}$$

The first term on the right-hand-side of the above equation represents the contribution by the area in intimate contact at the beginning of the bonding process. The initial area contact, $D_{ic}(0)$, can be obtained based on the fractal parameters of the tow surface, as discussed in ref. (9).

2.4 Nondimensional Analysis

The fusion bonding models in the previous sections suggest that the degree of bonding is a function of the material and processing parameters, i.e., temperature, pressure, time, viscosity, welding time, and surface roughness parameters. The influence of these parameters on the overall bonding process may be represented in terms of suitable dimensionless groups identified by means of a nondimensional analysis of the coupled bonding model, *Eq 19*, and the associated degree of healing and intimate contact functions given by *Eqs 17* and *18*, respectively.

For the purpose of the current analysis, the fusion bonding process is treated to be nonisothermal at a constant pressure. The expressions for the degree of healing and intimate contact are nondimensionalized by introducing a dimensionless temperature, θ, and a dimensionless time, τ, defined as follows:

$$\theta = \frac{T}{T_{ref}}; \quad \tau = \frac{t}{t_w^*(T_{ref})} \tag{20}$$

where T and T_{ref} are the actual temperature and the reference temperature (both in Kelvin), respectively, and t_w^* is the welding time at the reference temperature. Further, for long processing times, it is sufficient to retain only the first term within the square brackets in *Eq 18*, since it is dominant compared to unity, the second term. The expressions for the degrees of healing $[D_h(\tau)]$ and intimate contact $[D_{ic}(\tau)]$, are then obtained in terms of the dimensionless parameters as

$$D_h(\tau) = \left[\int_0^{\tau} \frac{1}{t'_w(\tau)} d\tau\right]^{1/4} \tag{21}$$

$$D_{ic}^{(n)}(\tau) = \mathbf{f_b} \cdot \frac{g(n)}{g(1)} \left[\int_{\tau_{n+1}}^{\tau} \frac{d\tau}{\mu'}\right]^{1/5};$$

$$\mathbf{f_b} = g(1)\left[\frac{t_w^* p_{app}}{\mu^*}\right]^{1/5}; \ \tau_{n+1} \le \tau \le \tau_n \tag{22}$$

where $g(n) = \frac{1}{f^n}\left[\frac{5}{4}\left(\frac{h_0}{L_0}\right)^2 \frac{f^{\frac{2nD}{2-D}+n+4}}{(f+1)^2}\right]^{\frac{1}{5}}$ is a geometric parameter characterizing the roughness of the asperity profile, and $g(1)$ is the geometric parameter corresponding to the first generation asperities, i.e., $n = 1$. Further, $t'_w = t_w(T)/t_w^*$, $\mu' = \mu(T)/\mu^*(T_{ref})$, and $\mathbf{f_b}$ is introduced as the *fusion bonding number*, which represents the ratio of the characteristic time for welding to that for intimate contact. Note that larger values of the fusion bonding number signify a rapid intimate contact development relative to healing, and conversely, a smaller value of $\mathbf{f_b}$ denotes rapid healing. Thus, the value of $\mathbf{f_b}$ can be used to determine the rate-limiting mechanism for the bonding process, as discussed in a later section on presentation of results.

Using the foregoing nondimensional relationships for the degrees of healing and intimate contact, the degree of bonding may be written in the form

$$D_b^{(n)}(\tau) = \mathbf{f_b} \int_0^{\tau}\left[\int_0^{\tau-\tau'} \frac{1}{t'_w} d\tau\right]^{1/4} \cdot \frac{d}{d\tau'}\left(\frac{g(n)}{g(1)}\left[\int_{\tau'_{n+1}}^{\tau'} \frac{d\tau}{\mu'}\right]^{1/5}\right) \cdot d\tau'; \ \tau_{n+1} \le \tau \le \tau_n \tag{23}$$

where the initial degree of intimate contact, $D_{ic}(0)$, is taken to be zero, which will yield a conservative estimate of the fusion bonding time.

3. EXPERIMENTAL STUDIES

The experimental studies presented in the paper are limited to the validation of the nonisothermal healing model since validation of the intimate contact model was considered in a previous study (8). The material used was a poly-ether-ether-ketone (PEEK) film with a thickness of 0.74 *mm* from Boedeker Plastics, Inc. The glass transition temperature and melting point of the film, as provided by the manufacturer, are 143°C and 338°C, respectively. A programmable Tetrahedron hot press was used in the fabrication of lap shear specimens. The press has two 254 × 254 *mm* platens with a force capacity of 5 tons and maximum temperature of 455°C. As-received PEEK film was cut into ribbons

and placed in the grooves of a steel mold. The gage length, the overlap length, and the width of the lap shear samples are 76.2 *mm*, 3.175 *mm*, and 6.35 *mm*, respectively.

The ribbons to be bonded were cleaned with acetone and care was taken to prevent the specimen surfaces from being contaminated. Further, to prevent the specimens from sticking to the mold, aluminum foil was used between the specimens and the grooves. Mold release agent is also applied between the specimens and the aluminum foil. The mold was placed in the Tetrahedron hot press programmed to yield desired temperature schedules, which are shown in the next section. Specimens were fabricated for several different bonding times within each schedule. To ensure good intimate contact between thermoplastic layers, the amount of pressure needed was calculated using the intimate contact model summarized in the previous section. A pressure of 40 *kPa* was found to be sufficient for the layers to achieve complete intimate contact within 10 seconds in all the cases. After the desired bonding time had elapsed, the mold was taken out of the hot press and quenched in cold water.

Lap shear testing was conducted at room temperature using an Instron tensile test machine, with a crosshead speed of 12.7 *mm/min*. Eight replicates were tested for each set of processing parameters. The shear strength was defined as the ratio of the fracture load to the lap area. The ultimate shear strength was determined by using long enough bonding time and was found to be 87.9 *MPa*, which is close to the ultimate bulk shear strength reported by the manufacturer. The degree of healing values were obtained as the ratio of instantaneous shear strength to the measured ultimate shear strength, and were used in the model validation studies discussed in the next section.

4. RESULTS AND DISCUSSION

In this section, validation of the nonisothermal healing model with experimental data is presented first. Parametric and model comparison studies are then discussed to illustrate the physical trends of the healing model. The coupled healing and intimate contact model is used to investigate the evolution of the degree of bonding, D_b, as function of the temperature schedules and the fusion bonding number.

Experimental validation of the healing model developed in this study was examined using the strength measurements on PEEK ribbons, as described previously. *Figure 3* shows the comparison of the model predictions with experimental data in terms of the degree of healing development with time under nonisothermal conditions. The temperature schedules used in the experiments have the ramp-up and hold stages, shown by the dashed lines in *Fig. 3*. The temperature-dependent welding time of PEEK used in the model predictions is given by the expression from Lee and Springer (4).

$$t_w = \left(\frac{1}{44.1}\ \exp\frac{3810}{T}\right)^4 \tag{24}$$

The numerical calculations of the healing development corresponding to the prescribed temperature variation were carried out until D_h reached a value of unity. Once a degree of healing of unity was achieved, the state of complete healing was preserved regardless of the further variation in the temperature schedule. The predictions of the current model are denoted in *Fig. 3* by the solid lines and the experimental data are represented by the symbols with the error bars. As the temperature gradient decreases from *Fig. 3a* to *Fig. 3b*, the healing development slows down as physically expected. Overall, a good agreement between the current model and the experimental data is observed for the nonisothermal schedules and through the entire healing process. More discussion on the validation of the healing model using other materials and processing conditions can be found in ref. (18).

With the validated healing model as basis, parametric effects and a comparison of the available models with the exact solution for nonisothermal healing are described in the following discussion. The parametric studies were conducted by considering nonisothermal variations of the form shown in *Fig. 4a*. The temperature schedules consisted of a linear ramp from T_0 to T_f within t_{ramp} seconds, following by a hold stage with a constant temperature T_f (*Fig. 4a*). The three parameters in the ramp-hold schedules are tabulated in *Fig. 4b*, which represent the temperature schedules used in the parametric and model comparison studies. In the following discussion, the temperature dependence of the welding time in *Eq 17* and the reptation time in *Eqs 5* and *6* are chosen to be that of the reptation time of AS4/PEEK reported in the literature (4). The choice of a single expression for the welding and reptation times serves as a common basis for the purpose of parametric studies and model comparison.

The influence of the temperature gradient on the healing development is shown in *Figs. 5a* and *5b*. The effect of positive temperature ramps ($dT/dt > 0$) where the temperature is increased from 380°C to 420°C in three different time durations, identified as Cases 1–3 in *Fig. 4b*, is illustrated in *Fig. 5a*. Since the reptation time decreases with increasing temperature, the healing development is accelerated with a steeper ramp. Consequently, as the temperature gradient increases from Case 3 to Case 1, the total time for achieving complete healing (i.e., $D_h = 1$) is seen to decrease in *Fig. 5a*. *Figure 5b* shows the effect of negative temperature ramps on the healing development. Again, the corresponding temperature history for each Case is given in *Fig. 4b*. Following a similar reasoning as for the heating cycles, the nature of the temperature dependence of the reptation time implies that a negative temperature ramp *decelerates* the healing process. This is evident in *Fig. 5b*, which shows that the time for realizing a given degree of

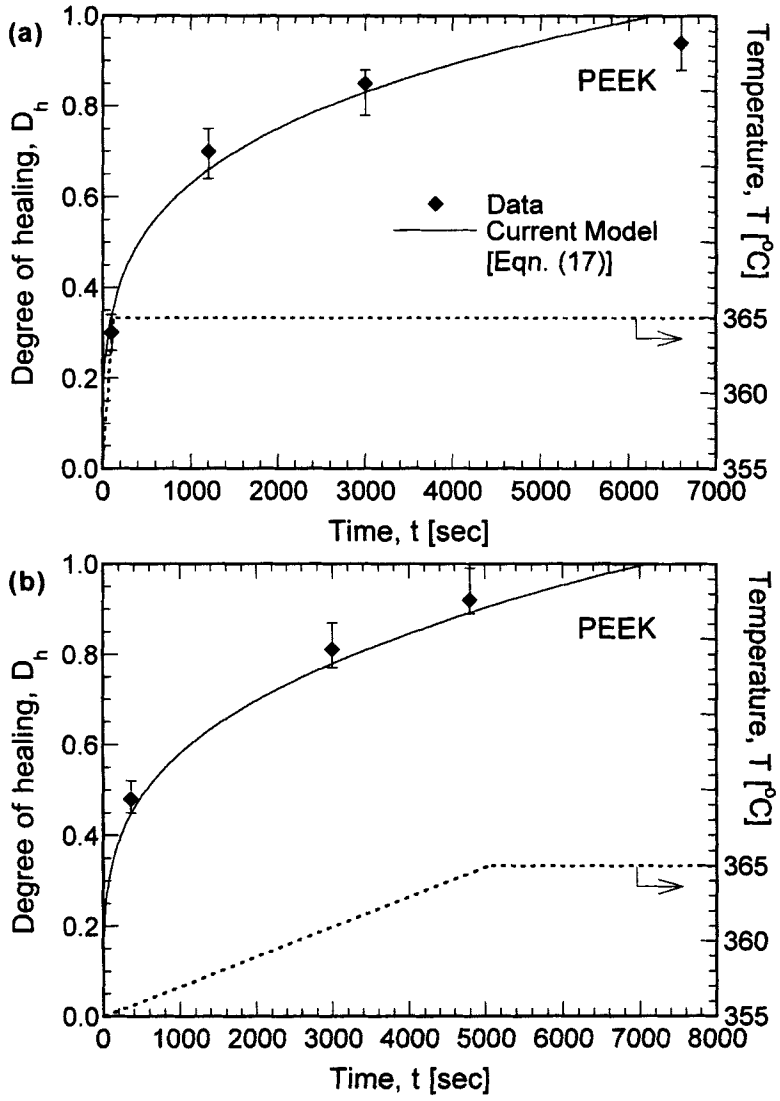

Fig. 3. Validation of the nonisothermal healing model (Eq 17) with experimental data on PEEK films.

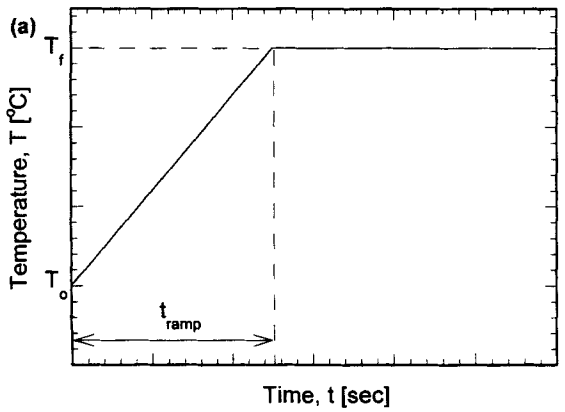

(b)

Case	T_0 [°C]	T_f [°C]	t_{ramp} [sec]
1	380	420	360
2	380	420	1800
3	380	420	3600
4	420	380	900
5	420	380	1800
6	420	380	5400
7	340	400	500
8	400	340	500

Fig. 4. (a) Schematic of the profile of the temperature variation and (b) values of the parameters of the temperature profile used in the parametric and model comparison studies.

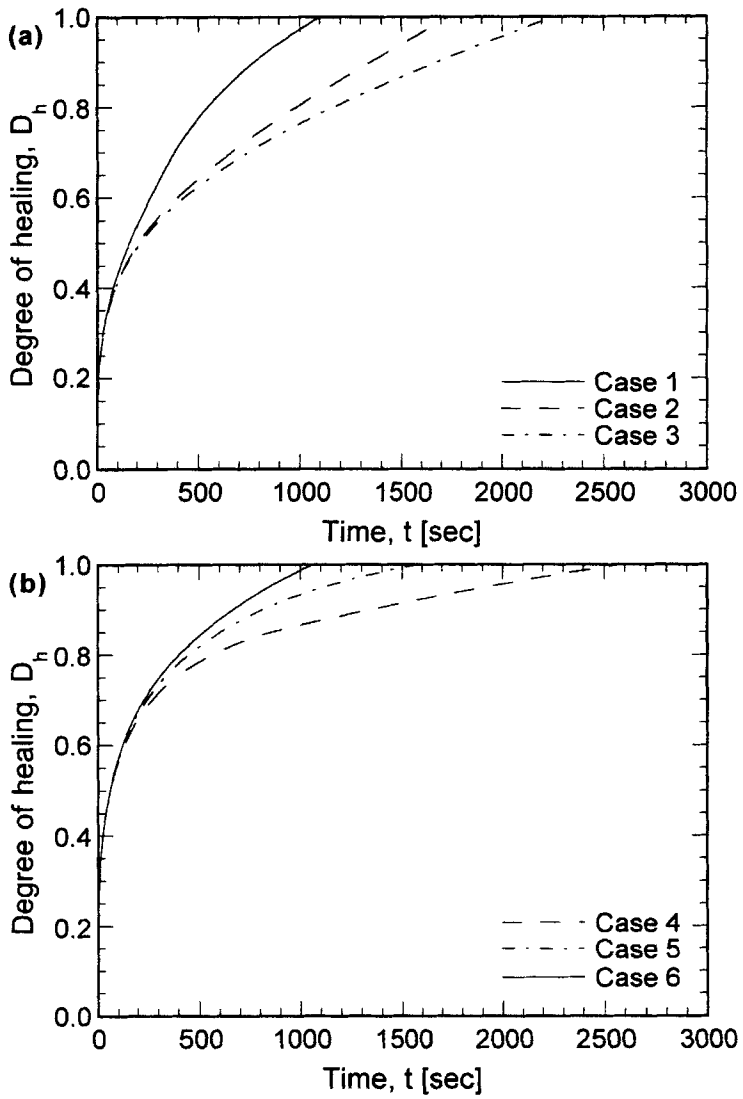

Fig. 5. Parametric studies showing the effects of the temperature and temperature gradient on the healing development, for (a) heating and (b) cooling of AS4/PEEK samples. The Case numbers pertain to the temperature profiles in Fig. 4.

healing decreases as the absolute value of the negative ramp decreases from Case 4 to Case 6.

In addition to the parametric study, the nonisothermal healing model was compared with the models presented by Bastien and Gillespie (12) and by Sonmez and Hahn (14), with the objective of ascertaining their accuracy relative to the exact model developed in this study. First, it is noted that all the nonisothermal models converge to the reptation model in *Eq 4* under isothermal conditions, whereas the predictions of the models are not identical under nonisothermal conditions. For the temperature histories considered in this paper, a time step of 0.1 second was found to yield converged numerical predictions for all the models.

Figure 6 compares the predictions of the different healing models for two temperature histories of the ramp-hold form illustrated in *Fig. 4a* and quantified as Case 7 and Case 8 in *Fig. 4b*. Case 7 corresponds to a steady heating from the melting point of AS4/PEEK (340°C) to the maximum temperature of 400°C with a ramp time of 500 seconds, and holding the temperature at 400°C until complete healing is attained, whereas, Case 8 represents a cooling schedule between the two temperatures, and with a ramp down time of 500 seconds. It is seen in *Fig. 6* that in the initial stages of the process all the models are comparable in predicting the healing development. However, in the case of the heating schedule (*Fig. 6a*), beyond about 30% healing, the models diverge in their estimate of the degree of healing. In particular, the model of Bastien and Gillespie predicts a considerably slower evolution of healing at the interface. The Sonmez and Hahn model also yields a smaller degree of healing at any instant during the process, although the deviation

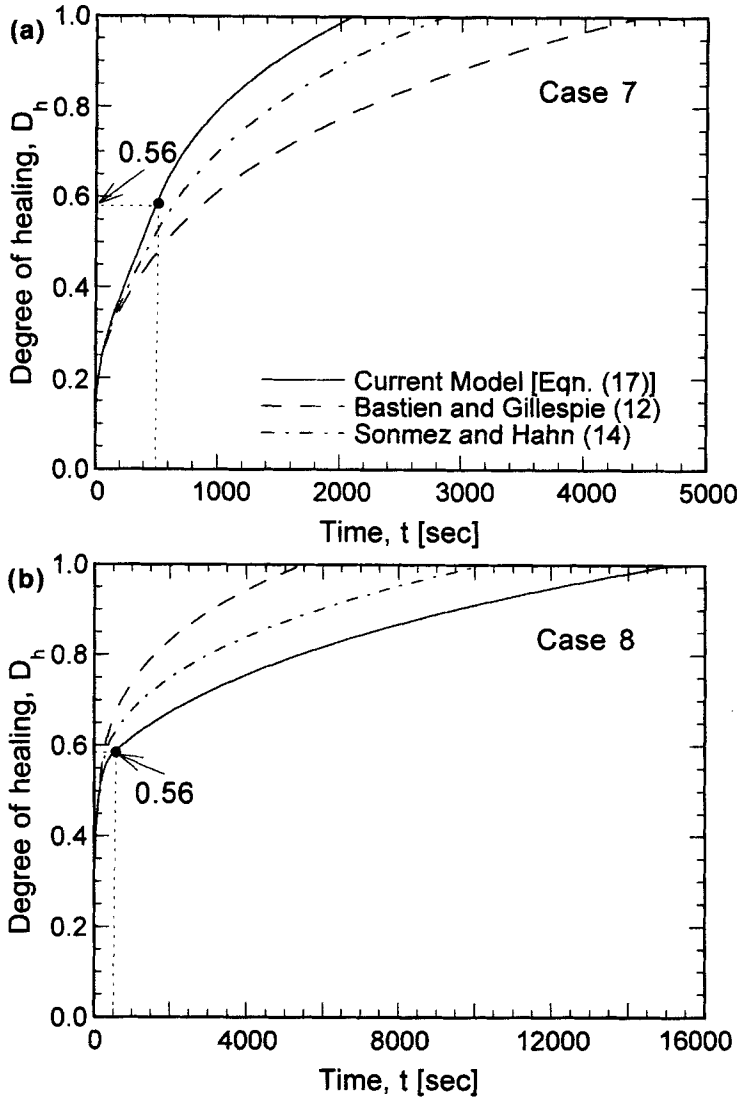

Fig. 6. Comparison of the nonisothermal model (Eq 17) with the models in the literature, for AS4/PEEK. Plots represents the degree of healing development for a heating cycle [Plot (a)], and a cooling cycle [Plot (b)].

from the exact solution is less than that for the Bastien and Gillespie model. For the temperature cycle represented by Case 7 (*Fig. 6a*), the healing time is significantly overestimated by more than a factor of two in the case of the Bastien and Gillespie model, and by about 33% in the case of the model of Sonmez and Hahn. *Figure 6b* shows the comparison for a cooling schedule with a negative ramp denoted by Case 8 in *Fig. 4b*. The relative trend among the models is converse to that seen in the case of the heating schedule in *Fig. 6a*. The model of Bastien and Gillespie and that of Sonmez and Hahn overpredict the healing development rates, with the healing times being 5,500 seconds and 10,000 seconds, respectively, in comparison to the value of 15,000 predicted by the exact solution.

It is interesting to note from the present healing model in *Figs. 6a* and *6b* that the degree of healing at the end of the linear ramp portions of the schedules, i.e., at t = 500 *sec.*, are identical (as marked in the plots) regardless of whether the material is heated from 340°C to 400°C in 500 seconds or cooled from 400°C to 340°C in 500 seconds. This is physically expected since the material is subject to the same temperature values except for the time during the linear schedule when the temperature is experienced. Furthermore, this physical consistency check elucidates an important distinction of the present model with respect to the other models which incorrectly predict a lower degree of healing at the end of a heating ramp and a higher degree of healing at the end of a cooling ramp. The models in the literature are therefore inconsistent with the physical healing process under nonisothermal conditions.

The foregoing discussion pertained to nonisothermal healing under assumption of complete interfacial area contact. In general, the bond strength development is a result of the coupled processes of healing and intimate contact, and the degree of bonding is

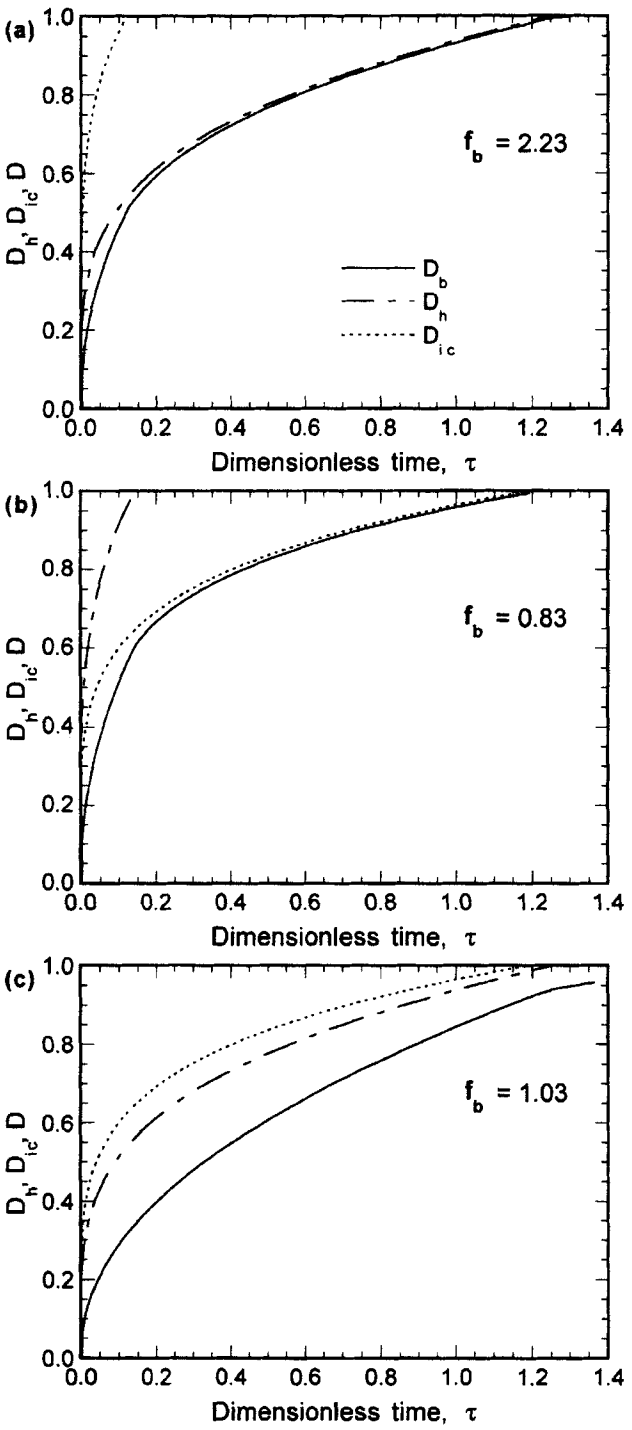

Fig. 7. Evolution of D_h, D_{ic}, and D_b with nondimensional time τ at three values of f_b to illustrate the influence of the fusion bonding number on the bond strength development.

given by the convolution of the intimate contact and healing development, as described in the previous section (*Eq 23*). The results presented in the remainder of this section examine the coupling between the two mechanisms under nonisothermal conditions.

Figures 7a–c compare the evolutions of D_h, D_{ic}, and D_b with the nondimensional time τ (defined by *Eq 20*) at three values of the fusion bonding number, f_b. The following parameters are used in the numerical calculations: 1) the reference temperature, T_{ref} = 365°C, 2) the viscosity and welding time of polymer AS4/PEEK reported by Lee and Springer (4), 3) the temperature schedule in *Fig. 3b*, and 4) the geometric parameters of AS4/PEEK surface given by Yang and Pitchumani (8). In general, the bonding process can be healing controlled, intimate contact controlled, or equally dominated by both mechanisms, depending on the value of f_b. Since f_b determines the ratio of the characteristic time for welding to that for intimate contact, a large value of f_b (> 1) corresponds to a long welding time and a short intimate contact time, indicating a healing controlled process. This scenario is represented in *Fig. 7a*, which corresponds to a f_b value of 2.23. In this case, the time for complete intimate contact is τ = 0.12 while that for complete healing is τ = 1.25, and the time for achieving full bonding is τ = 1.29. The degree of bonding curve is seen to closely follow the degree of healing curve, and the final bonding time can be estimated to a reasonable degree of accuracy as that of healing.

Following a similar reasoning, f_b < 1 indicates an intimate-contact-controlled process where the characteristic time for intimate contact is much longer than that for healing. *Figure 7b*, with a f_b value of 0.83, exemplifies an intimate-contact-limited processing wherein the dimensionless times for intimate contact, healing, and bonding are 1.18, 0.15, and 1.22, respectively. It is seen that the evolution of the degree of bonding and the bonding time can be estimated quite accurately as those corresponding to the intimate contact process. When the value of f_b is close to unity, both healing and intimate contact processes have comparable time scales, and the bond strength development is equally dominated by both these mechanisms, as illustrated by *Fig. 7c*. The evolution of the D_b can not be estimated by D_h or D_{ic} individually, and the convolution integral, *Eq 23*, has to be evaluated to obtain the bonding development and the time for complete bonding.

The results presented in *Fig. 7* qualitatively establish the three processing regimes namely, healing-limited, intimate-contact-limited, and healing and intimate contact being equally dominant. However, from a process design viewpoint, it will be useful to derive quantitative ranges of values of f_b corresponding to each of the three regimes. To this end, *Fig. 8a* presents two process time ratios, τ_b/τ_w and τ_b/τ_{ic}, as functions of the fusion bonding number, where τ_b, τ_w, and τ_{ic} are dimensionless times required to achieve complete bonding, welding, and intimate contact, respectively. The numerical calculations used the same parameters as those in *Fig. 7*, except for the temperature schedule parameters. The temperature schedule followed the ramp-and-hold profile shown in *Fig. 4a*, in which the dimensionless temperatures at the beginning and end of the ramp were θ_0 = 0.976 and θ_f = 1.086, based on the T_{ref} value mentioned previously, and ramp

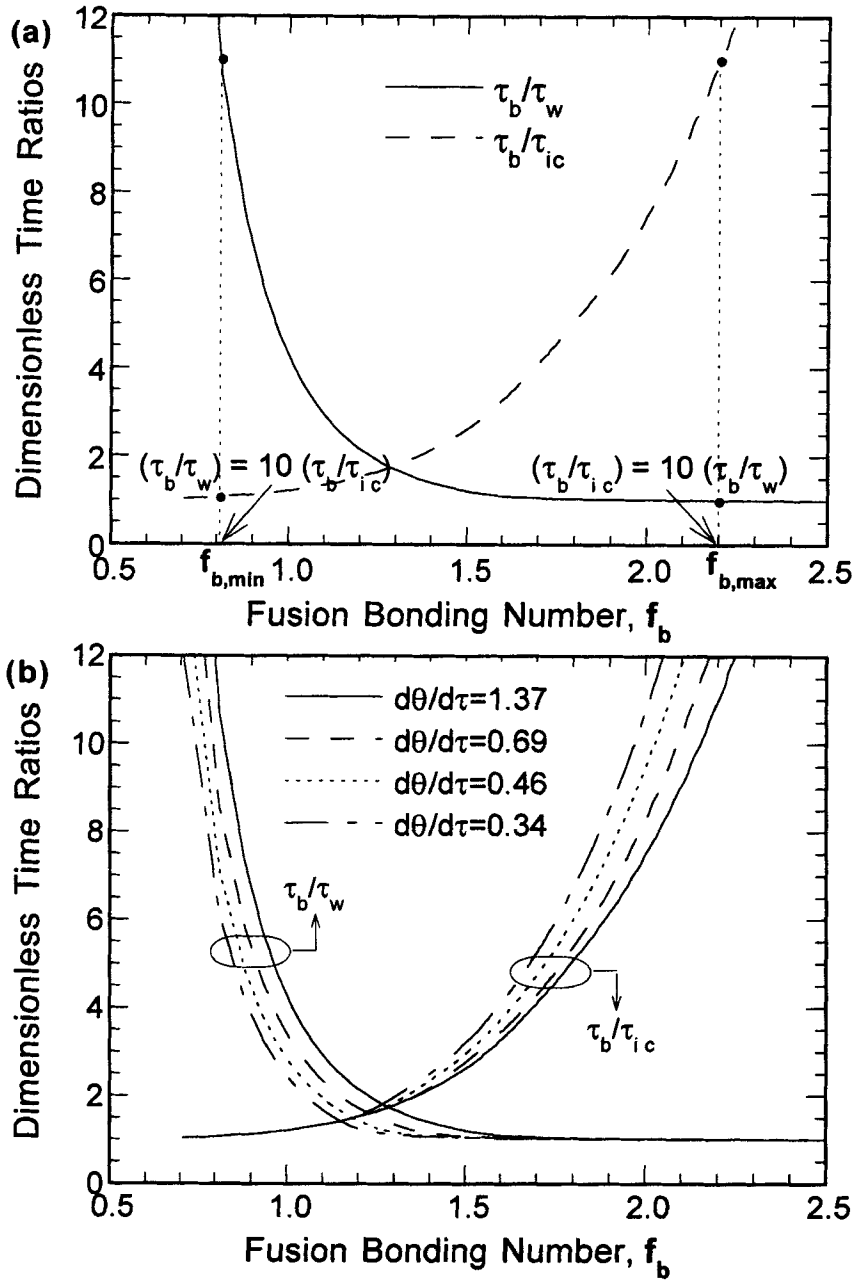

Fig. 8. (a) Variation of the time ratios, τ_b/τ_w and τ_b/τ_{ic}, with the fusion bonding number and (b) the influence of the temperature gradient on the variation.

time was such that the dimensionless temperature gradient, $\frac{d\theta}{d\tau} = 1.37$.

It is seen in *Fig. 8a* that as the fusion bonding number increases, the τ_b/τ_w ratio decreases whereas the τ_b/τ_{ic} ratio increases. An increase in the fusion bonding number, $\mathbf{f_b}$, denotes an increase in the welding time relative to the intimate contact time, or equivalently, the intimate contact process being faster than the healing process. Consequently, the time for intimate contact decreases while the welding time increases, which is reflected in the increase in τ_b/τ_{ic} and the decrease in τ_b/τ_w with increasing $\mathbf{f_b}$. In the limit of $\mathbf{f_b} \to 0$, the healing process is instantaneously completed, i.e., $\tau_w \to 0$, and τ_b/τ_w approaches infinity, which is evident in the sharp increase in the τ_b/τ_w curve for small values of $\mathbf{f_b}$. Also, owing to the instantaneous healing, the ratio of τ_b to τ_{ic} approaches unity as $\mathbf{f_b} \to 0$. On the other hand, in the limit of $\mathbf{f_b} \to \infty$, the time for achieving complete interfacial contact is zero, and the bonding process is limited by the healing development. As a result, $\tau_b/\tau_w \to 1$, while the ratio of τ_b to τ_{ic} tends to infinity, as seen in *Fig. 8a*.

Based on the variation of τ_b/τ_{ic} seen in *Fig. 8a* it is evident that a critical value $\mathbf{f_{b,min}}$ may be identified such that for $\mathbf{f_b} < \mathbf{f_{b,min}}$, the bond strength evolution can be accurately estimated using the intimate contact model. The critical value $\mathbf{f_{b,min}}$ is defined here as the value of $\mathbf{f_b}$ for which the intimate contact process takes an order of magnitude longer to complete relative to the welding time, i.e., $\left[\frac{\tau_b}{\tau_w}\right]/\left[\frac{\tau_b}{\tau_{ic}}\right] = 10$. The region $\mathbf{f_b} < \mathbf{f_{b,min}}$ therefore constitutes the intimate-contact-limited processing regime. Similarly, the τ_b/τ_w variation with $\mathbf{f_b}$ in *Fig. 8a* suggests that a critical value $\mathbf{f_{b,max}}$ exists such that for $\mathbf{f_b} > \mathbf{f_{b,max}}$ the bonding process is healing-limited. The value of $\mathbf{f_{b,max}}$ corresponds to the fusion bonding number at which healing time is an order of magnitude larger than the time to achieve intimate contact, i.e., $\left[\frac{\tau_b}{\tau_{ic}}\right]/\left[\frac{\tau_b}{\tau_w}\right] = 10$. For the data presented in *Fig. 8a*, corresponding to a dimensionless temperature gradient $d\theta/d\tau = 1.37$, the values of $\mathbf{f_{b,min}}$ and $\mathbf{f_{b,max}}$ are 0.82 and 2.16, respectively. In the range $\mathbf{f_{b,min}} < \mathbf{f_b} < \mathbf{f_{b,max}}$, the healing and intimate contact mechanisms are equally dominant in governing the interfacial bond strength development.

Figure 8b examines the effect of the temperature gradient on the variation of τ_b/τ_{ic} and τ_b/τ_w with the fusion bonding number. It is seen that while the monotonically decreasing (τ_b/τ_w) and monotonically increasing (τ_b/τ_{ic}) trends with $\mathbf{f_b}$ are preserved for each temperature gradient, both curves shift to the left as the temperature gradient decreases. These trends may be explained as follows. Since the temperature schedules considered are all above the melting point of the material, the change in time for intimate contact with temperature gradient is relatively small. However, the healing process slows down as temperature gradient decreases, and the welding time increases which causes the decrease of the ratio τ_b/τ_w for a given value of $\mathbf{f_b}$. The increase of welding time yields longer bonding time, which is the reason for the increase of the ratio τ_b/τ_{ic} as the temperature gradient decreases. The critical values $\mathbf{f_{b,min}}$ and $\mathbf{f_{b,max}}$ may be determined for each temperature gradient, as explained above with reference to *Fig. 8a*.

The variation of the bounding parameters, $\mathbf{f_{b,min}}$ and $\mathbf{f_{b,max}}$, with the temperature gradient are presented in *Fig. 9* to identify the three processing regimes for the AS4/PEEK material for various heating and cooling rates in the nonisothermal schedule. *Figure 9a* shows the regimes for heating schedules, where it is seen that the critical values, $\mathbf{f_{b,min}}$ and $\mathbf{f_{b,max}}$, both increase with the temperature gradient. This is consistent with the shift in the curves with temperature gradient noted in *Fig. 8b*. Further, for large temperature gradient, the $\mathbf{f_{b,min}}$ and $\mathbf{f_{b,max}}$ values are nearly constants, such that $\mathbf{f_b} < 0.85$ represents the intimate-contact-limited processing, $\mathbf{f_b} > 2.14$ denotes a healing-limited processing, while for $0.85 < \mathbf{f_b} < 2.14$, the nonisothermal bonding process is equally dominated by healing and intimate contact development. The processing regimes in the case of ramp-and-hold cooling schedules between $\theta_0 = 1.086$ and $\theta_f = 0.976$ with varying cooling rates are shown in *Fig. 9b*. In the case of varying cooling rates, the τ_b/τ_w and τ_b/τ_{ic} curves shift to the right with decreasing magnitude of the cooling rate. As a result, the critical values, $\mathbf{f_{b,min}}$ and $\mathbf{f_{b,max}}$, decrease with increasing magnitude of the cooling rate, as seen in *Fig. 9b*. As in the case of the heating schedules, the values of $\mathbf{f_{b,min}}$ and $\mathbf{f_{b,max}}$ each approach a constant value for higher cooling rates, such that $\mathbf{f_b} < 0.61$ and $\mathbf{f_b} > 1.46$, respectively, denote the intimate-contact-limited and the healing-limited regimes, while values of $\mathbf{f_b}$ between these limits represent the equally dominated processing regime.

The processing regimes identified in *Figs. 9a* and *9b* serve as useful design tool for determining the controlling mechanisms for a given combination of temperature gradient and fusion bonding number. This information, together with the models presented in this paper, will in turn enable an accurate design of the process parameters for an application. It must be mentioned that the processing regimes identified pertain to the AS4/PEEK material, and the quantitative values of $\mathbf{f_{b,min}}$ and $\mathbf{f_{b,max}}$ may be different for other materials. However, the overall methodology and the general trends elucidated in this article are broadly relevant.

5. CONCLUSIONS

A nonisothermal model of healing evolution during thermoplastic fusion bonding was developed based on first principles formulation of the polymer reptation process, and the model was validated by experimental data on thermoplastic polymer PEEK. Parametric studies were presented to show the effects of temperature history on the degree of healing evolution with time. Comparison of the nonisothermal healing model with the models of Bastien and Gillespie (12) and Sonmez and Hahn (14), which are based on approximate extensions of the isothermal reptation model, revealed that the models in the literature could lead to considerable inaccuracies in the estimation of interfacial strength. The healing model was coupled with an intimate contact model in the literature to evaluate the degree of bonding evolution with time under nonisothermal conditions. It was shown that a dimensionless fusion bonding number, $\mathbf{f_b}$, can be used to identify three processing regimes, namely, intimate-contact-controlled ($\mathbf{f_b} < \mathbf{f_{b,min}}$), healing-controlled ($\mathbf{f_b} > \mathbf{f_{b,max}}$), and the regime equally dominated by both mechanisms ($\mathbf{f_{b,min}} < \mathbf{f_b} < \mathbf{f_{b,max}}$). The bounding parameters, $\mathbf{f_{b,min}}$ and $\mathbf{f_{b,max}}$, were developed for the thermoplastic prepreg material AS4/PEEK, as function of the heating and cooling rates in the nonisothermal schedule. The processing regimes and the models provided in this study serve as a design tool for determining the controlling mechanisms and the evaluation of the interlaminar bond strength development during processing.

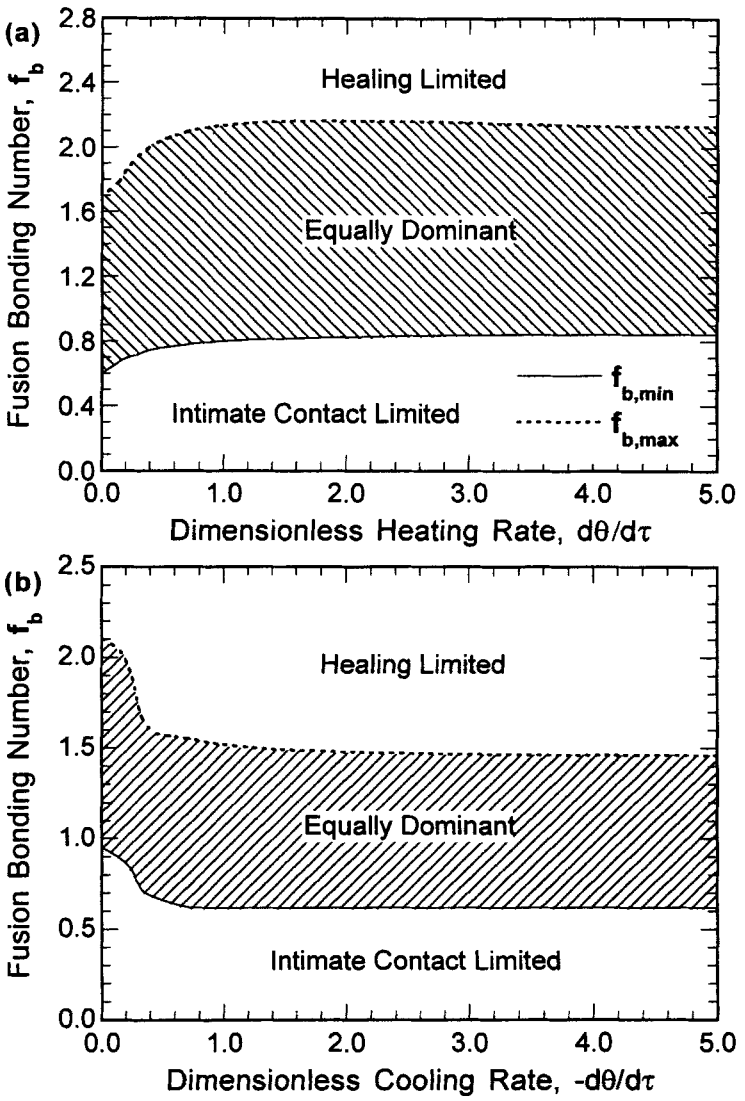

Fig. 9. Processing regimes identifying the controlling mechanisms during the manufacturing process of AS4/PEEK as a function of the fusion bonding number, for (a) heating and (b) cooling temperature schedules.

ACKNOWLEDGMENTS

The work reported in this paper was funded by the National Science Foundation (Grant No. CTS-9912093). We gratefully acknowledge their support.

NOMENCLATURE

D = reptation diffusion coefficient, $[m^2/s]$; fractal dimension of thermoplastic surfaces
D_0 = isothermal reptation diffusion coefficient at temperature T_0, $[m^2/s]$
D_b = degree of bonding
D_h = degree of healing based on interfacial strength
D_{ic} = degree of intimate contact
f = function defined in the model development for brevity (*Eq 15*); aspect ratio of asperities in a Cantor set geometry
$\mathbf{f_b}$ = fusion bonding number
$g(n)$ = geometric parameter characterizing the roughness of the asperity profile
$g(1)$ = geometric parameter corresponding to the first generation asperities
h_0 = recess depth of the first generation asperities, $[m]$
h_n = recess depth of the $(n-1)$th generation asperities, $[m]$
L = total length of a polymer chain, $[m]$
ℓ = instantaneous minor chain length, $[m]$
L_0 = total horizontal length of the Cantor set block, $[m]$
L_n = total horizontal length of the (n)th generation asperities, $[m]$
L_w = minor chain length at the welding time, $[m]$
M = polymer molecular weight, $[kg/kmol]$
M_c = critical entanglement molecular weight, $[kg/kmol]$

P = probability density function, $[m^{-1}]$
p_{app} = applied consolidation pressure, $[N/m^2]$
s = curvilinear coordinate along the encompassing tube, $[m]$
T = temperature, $[K]$
T_{ref} = reference temperature, $[K]$
t = time, $[s]$
t_b = time required to achieve complete bonding, $[s]$
t_{ic} = time required to achieve complete intimate contact, $[s]$
t_n = end time for the consolidation process of the (n)th generation asperities, $[s]$
t_R = reptation time of a thermoplastic material, $[s]$
t_w = time required to achieve complete welding, $[s]$
t_w^* = welding time at the reference temperature, $[s]$
t_w' = dimensionless welding time
u_n = cumulative displacement of the flattening of asperities of generation $\geq n$, $[m]$

Greek symbols

χ = interpenetration distance, $[m]$
χ_w = interpenetration distance at the welding time, $[m]$
χ_∞ = maximum interpenetration distance, $[m]$
δ = Dirac delta function, $[m^{-1}]$
μ = viscosity of the thermoplastic material, $[Ns/m^2]$
μ^* = viscosity of the thermoplastic material at the reference temperature, $[Ns/m^2]$
μ' = dimensionless viscosity of the thermoplastic material
θ = dimensionless temperature
σ = interlaminar bond strength, $[MPa]$
σ_∞ = ultimate interlaminar bond strength, $[MPa]$
τ = dimensionless time
τ_b = dimensionless bonding time
τ_{ic} = dimensionless intimate contact time
τ_w = dimensionless welding time

REFERENCES

1. R. P. Wool, B. L. Yuan, and O. J. McGarel, *Polym. Eng. Sci.*, **29**, 1340 (1989).
2. R. P. Wool and K. M. O'Connor, *J. Appl. Phys.*, **52**, 5953 (1981).
3. Y. H. Kim and R. P. Wool, *Macromolecules*, **16**, 1115 (1983).
4. W. I. Lee and G. S. Springer, *J. Composite Mater.*, **21**, 1017 (1987).
5. R. Pitchumani *et al.*, *Int. J. Heat Mass Transfer*, **39**, 1883 (1996).
6. C. A. Butler, R. L. McCullough, R. Pitchumani, and J. W. Gillespie, Jr., *J. Thermoplastic Composite Mater.*, **11**, 338 (1998).
7. P. H. Dara and A. C. Loos, "Thermoplastic Matrix Composite Processing Model," Virginia Polytechnic Institute Report, CCMS-85-10, (1985) Hampton, VA.
8. F. Yang and R. Pitchumani, *J. Mater. Sci.*, **36**, 4661 (2001).
9. F. Yang and R. Pitchumani, *Polym. Eng. Sci.*, **42**, 424 (2002).
10. P. G. deGennes, *J. Chemical Phys.*, **55**, 572 (1971).
11. S. Prager and M. Tirrell, *J. Chemical Phys.*, **75**, 5194 (1981).
12. L. J. Bastien and J. W. Gillespie, Jr., *Polym. Eng. Sci.*, **31**, 1720 (1991).
13. C. Ageorges, L. Ye, and M. Hou, *Composites: Part A*, **32**, 839 (2001).
14. F. O. Sonmez and H. T. Hahn, *J. Thermoplastic Composite Mater.*, **10**, 543 (1997).
15. R. P. Wool, *Polymer Interfaces, Structure and Strength*, p. 74, Hanser Publishers, Munich, Vienna, New York (1995).
16. C. W. Macosko, *Rheology Principles, Measurements, and Applications*, p. 502, Wiley-VCH, Inc., New York City (1994).
17. E. Kreyszig, *Advanced Engineering Mathematics*, Wiley, Sixth Edition (1988).
18. F. Yang and R. Pitchumani, *Macromolecules*, **35**, 3213 (2002).
19. F. Yang, *Investigations on Interface and Interphase Development in Polymer-Matrix Composite Materials*, Ph.D. Thesis, Department of Mechanical Engineering, University of Connecticut (2002).